PHYSICAL REVIEW D **83,** 054009 (2011)

Analytic solution to leading order coupled DGLAP evolution equations: A new perturbative QCD tool

Martin M. Block
Department of Physics and Astronomy, Northwestern University, Evanston, Illinois 60208, USA

Loyal Durand
Department of Physics, University of Wisconsin, Madison, Wisconsin 53706, USA

Phuoc Ha
Department of Physics, Astronomy and Geosciences, Towson University, Towson, Maryland 21252, USA

Douglas W. McKay
Department of Physics and Astronomy, University of Kansas, Lawrence, Kansas 66045, USA
(Received 12 October 2010; published 7 March 2011)

We have analytically solved the LO perturbative QCD singlet DGLAP equations [V. N. Gribov and L. N. Lipatov, Sov. J. Nucl. Phys. **15**, 438 (1972)][G. Altarelli and G. Parisi, Nucl. Phys. **B126**, 298 (1977)][Y. L. Dokshitzer, Sov. Phys. JETP **46**, 641 (1977)] using Laplace transform techniques. Newly developed, highly accurate, numerical inverse Laplace transform algorithms [M. M. Block, Eur. Phys. J. C **65**, 1 (2010)][M. M. Block, Eur. Phys. J. C **68**, 683 (2010)] allow us to write fully decoupled solutions for the singlet structure function $F_s(x, Q^2)$ and $G(x, Q^2)$ as $F_s(x, Q^2) = \mathcal{F}_s(F_{s0}(x_0), G_0(x_0))$ and $G(x, Q^2) = \mathcal{G}(F_{s0}(x_0), G_0(x_0))$, where the x_0 are the Bjorken x values at Q_0^2. Here $\mathcal{F}_s$ and $\mathcal{G}$ are known functions—found using LO DGLAP splitting functions—of the initial boundary conditions $F_{s0}(x) \equiv F_s(x, Q_0^2)$ and $G_0(x) \equiv G(x, Q_0^2)$, i.e., the chosen starting functions at the virtuality Q_0^2. For both $G(x)$ and $F_s(x)$, we are able to *either devolve or evolve* each separately and rapidly, with very high numerical accuracy—a computational fractional precision of $O(10^{-9})$. Armed with this powerful new tool in the perturbative QCD arsenal, we compare our numerical results from the above equations with the published MSTW2008 and CTEQ6L LO gluon and singlet F_s distributions [A. D. Martin, W. J. Stirling, R. S. Thorne, and G. Watt, Eur. Phys. J. C **63**, 189 (2009)], starting from their initial values at $Q_0^2 = 1$ GeV^2 and 1.69 GeV^2, respectively, using their choice of $\alpha_s(Q^2)$. This allows an important independent check on the accuracies of their evolution codes and, therefore, the computational accuracies of their published parton distributions. Our method completely decouples the two LO distributions, at the same time guaranteeing that both G and F_s satisfy the singlet coupled DGLAP equations. It also allows one to easily obtain the effects of the starting functions on the evolved gluon and singlet structure functions, as functions of both Q^2 and Q_0^2, being equally accurate in devolution ($Q^2 < Q_0^2$) as in evolution ($Q^2 > Q_0^2$). Further, it can also be used for nonsinglet distributions, thus giving LO analytic solutions for individual quark and gluon distributions at a given x and Q^2, rather than the numerical solutions of the coupled integral-differential equations on a large, but fixed, two-dimensional grid that are currently available.

DOI: 10.1103/PhysRevD.83.054009 PACS numbers: 12.38.−t, 12.38.Bx

I. INTRODUCTION

The search for new physics at the LHC demands an accurate knowledge of gluon distribution functions at small Bjorken x and large virtuality Q^2, both for estimating QCD backgrounds and for calculating gluon-initiated processes. The traditional method has simultaneously determined gluon and quark distribution functions by fitting experimental data on neutral- and charged-current deep inelastic scattering processes and some jet data over a large domain of values of x and Q^2. The distributions at small x and large Q^2 are determined mainly by the proton structure function $F_2^{\gamma p}(x, Q^2)$ measured in deep inelastic ep (or $\gamma^* p$) scattering. The fitting process starts with an initial Q_0^2, typically less than or equal to the square of the c quark mass, $m_c^2 \approx 2$ GeV^2, and individual quark and gluon trial distributions parametrized with predetermined shapes, given as functions of x for the chosen Q_0^2. The distributions are then evolved numerically on a finite, albeit large, two-dimensional grid in x and Q^2 to larger Q^2 using the coupled integral-differential DGLAP equations [1–3], typically in LO and next-to-leading order (NLO), and the results used to predict measured quantities. The final distributions are then determined by adjusting the input parameters to obtain a best fit to experimental data, fitting both HERA and Tevatron data over a large range of x and Q^2, along with selected hard scattering data from fixed target experiments. This procedure is very indirect in the case of the gluon: the gluon distribution $G(x, Q^2) = xg(x, Q^2)$ does not

contribute directly to the accurately determined structure function $F_2^{\gamma p}(x, Q^2)$, and it is determined only through the quark distributions in conjunction with the evolution equations, or at large x, from jet data. For recent determinations of the gluon and quark distributions, see [4–9].

In the following, we will summarize our method for analytically determining $G(x, Q^2)$ and the singlet structure function $F_s(x, Q^2)$ *directly* and *individually*, using as input $G_0(x) \equiv G(x, Q_0^2)$ and $F_{s0}(x) \equiv F_s(x, Q_0^2)$, where Q_0^2 is arbitrary, with the guarantee that each distribution individually satisfies the coupled DGLAP equations. The method is readily extended to embrace nonsinglet functions, so that it can be used also to find individual quark distributions. However, we will not pursue that goal in this communication. Instead, we give a numerical demonstration which takes advantage of the fact that our analytic solutions achieve numerical accuracies of $O(10^{-9})$, giving us a new diagnostic tool to verify *published* LO singlet structure functions $[F_s(x, Q^2)]$ and gluon $[G(x, Q^2) = xg(x, Q^2)]$ distributions. In order to test the numerical accuracy of their evolution codes, we consider two cases, using the published LO starting distributions for G_0 and F_{s0}:

(1) MSTW2008 [4]: for $Q_0^2 = 1$ GeV^2, we generate LO singlet structure functions and gluon distributions [4], using the strong coupling constant $\alpha_s(Q^2)$ that they used for their LO evolution, and compare them with their published values MSTW2008 [4] for the domain $10^{-6} \leq x \leq 1$ and $1 \leq Q^2 \leq 100\,000$. We find that their evolution code has serious problems at small x, producing significant numerical inaccuracies. It should be noted that the MSTW group *does not* do devolution.

(2) CTEQ6L [5]: for $Q_0^2 = 1.69$ GeV^2, we generate LO singlet structure functions and gluon distributions, using the strong coupling constant $\alpha_s(Q^2)$ [6] they used for both LO evolution and devolution. With our high numerical precision at *all* x and Q^2, we are able to verify all of their published *evolution* results—to larger Q^2—but show that their published *devolution* results, i.e., $Q^2 < Q_0^2$, have significant numerical inaccuracies at small x.

Finally, using our accurate CTEQ devolution results, we compare LO starting distributions for both groups at $Q^2 = 1$ GeV^2, noting that the CTEQ6L LO gluon distribution turns over and becomes negative at small x, i.e., $x \lesssim 5 \times 10^{-5}$, whereas the MSTW2008 LO gluon starting distribution continues to rise sharply at small x.

II. DECOUPLING THE COUPLED LO SINGLET DGLAP EQUATIONS

Our approach uses a somewhat unusual application of Laplace transforms [10,11], in which we first introduce the variable $\upsilon \equiv \ln(1/x)$ into the coupled DGLAP equations, then Laplace transform these coupled integral-differential equations in υ space to obtain coupled homogeneous first-order differential equations in the Laplace-space variable s. We solve these equations analytically. Finally, using fast and accurate numerical inverse Laplace transform algorithms [12,13], we transform the solutions back into υ space, and, finally, into Bjorken x space, so that we can write

$$F_s(x, Q^2) = \mathcal{F}_s(F_{s0}(x_0), G_0(x_0)) \quad \text{and}$$
$$G(x, Q^2) = \mathcal{G}(F_{s0}(x_0), G_0(x_0)), \tag{1}$$

where the functions $\mathcal{F}$ and $\mathcal{G}$ are determined by the splitting functions in the DGLAP equations, with x_0 being the Bjorken x at the starting virtuality Q_0^2; $F_{s0}(x)$ and $G_0(x)$ are the known starting distributions at $Q^2 = Q_0^2$, where evolution (devolution) begins.

Our method can be generalized to NLO (see Ref. [14]), but for brevity, we will limit ourselves to LO in this paper. We write the coupled LO DGLAP equations [10,11] as

$$\begin{aligned}
&\frac{4\pi}{\alpha_s(Q^2)} \frac{\partial F_s}{\partial \ln Q^2}(x, Q^2) \\
&\quad = 4F_s(x, Q^2) + \frac{16}{3} F_s(x, Q^2) \ln\frac{1-x}{x} \\
&\qquad + \frac{16}{3} x \int_x^1 \left(\frac{F_s(z, Q^2)}{z} - \frac{F_s(x, Q^2)}{x}\right) \frac{dz}{z-x} \\
&\qquad - \frac{8}{3} x \int_x^1 F_s(z, Q^2) \left(1 + \frac{x}{z}\right) \frac{dz}{z^2} \\
&\qquad + 2n_f x \int_x^1 G(z, Q^2) \left(1 - 2\frac{x}{z} + 2\frac{x^2}{z^2}\right) \frac{dz}{z^2},
\end{aligned} \tag{2}$$

$$\begin{aligned}
&\frac{4\pi}{\alpha_s(Q^2)} \frac{\partial G}{\partial \ln Q^2}(x, Q^2) \\
&\quad = \frac{33 - 2n_f}{3} G(x, Q^2) + 12 G(x, Q^2) \ln\frac{1-x}{x} \\
&\qquad + 12x \int_x^1 \left(\frac{G(z, Q^2)}{z} - \frac{G(x, Q^2)}{x}\right) \frac{dz}{z-x} \\
&\qquad + 12x \int_x^1 G(z, Q^2) \left(\frac{z}{x} - 2 + \frac{x}{z} - \frac{x^2}{z^2}\right) \frac{dz}{z^2} \\
&\qquad + \frac{8}{3} \int_x^1 F_s(z, Q^2) \left(1 + \left(1 - \frac{x}{z}\right)^2\right) \frac{dz}{z}.
\end{aligned} \tag{3}$$

Here $\alpha_s(Q^2)$ is the running strong coupling constant, and for LO MSTW2008 [4] is given by the LO form

$$\alpha_s(Q^2) = \frac{4\pi}{(11 - \frac{2}{3} n_f) \ln(Q^2/\Lambda_{n_f}^2)}, \tag{4}$$

with n_f the number of quark flavors. The QCD parameter Λ_5 is fixed so that the known $\alpha_s(M_Z^2)$ is reproduced, and then Λ_4 and Λ_3 are adjusted so that α_s is continuous across the boundaries $Q^2 = M_b^2$ and M_c^2, respectively, where M_b and M_c are the masses of the b and c quarks. Later, we will

also introduce the NLO form of α_s used [with $\alpha_s(M_Z^2) = 0.118$] in their LO CTEQ6L [5] evolution, when we discuss CTEQ6L parton distributions functions.

We now examine the last term of line 2 and the term in line 3 in Eq. (2) (the two terms that begin with the factor 16/3), and rewrite them, introducing the variable changes $v = \ln(1/x)$, $w = \ln(1/z)$, and the notation $\hat{F}_s(v, Q^2) \equiv F_s(e^{-v}, Q^2)$, $\hat{G}(v, Q^2) \equiv G(e^{-v}, Q^2)$, as

$$\begin{aligned}&\frac{16}{3}\hat{F}_s(v, Q^2)\ln(e^v - 1) + \frac{16}{3}\int_0^v (\hat{F}_s(w, Q^2) \\ &\quad - \hat{F}_s(v, Q^2)e^{v-w})\frac{1}{e^{v-w} - 1}dw \\ &= \frac{16}{3}\int_0^v \frac{\partial \hat{F}_s}{\partial w}(w, Q^2)\ln(1 - e^{-(v-w)})dw, \end{aligned} \tag{5}$$

where the final result—the last line in Eq. (5)—is found by replacing the upper limit v in the integral of line 1 of Eq. (5) by $v - \epsilon$, carrying out the integrals, doing a partial integration and, finally, taking the limit as $\epsilon \to 0$. Similarly, we find for the last two terms of line 1 in Eq. (3) that

$$\begin{aligned}&12\hat{G}(v, Q^2)\ln(e^v - 1) + 12\int_0^v (\hat{G}(w, Q^2) \\ &\quad - \hat{G}(v, Q^2)e^{v-w})\frac{1}{e^{v-w} - 1}dw \\ &= 12\int_0^v \frac{\partial \hat{G}}{\partial w}(w, Q^2)\ln(1 - e^{-(v-w)})dw. \end{aligned} \tag{6}$$

We now rewrite Eqs. (2) and (3) in terms of the new variable v as

$$\begin{aligned}&\frac{4\pi}{\alpha_s(Q^2)}\frac{\partial \hat{F}_s}{\partial \ln Q^2}(v, Q^2) \\ &= 4\hat{F}_s(v, Q^2) + \frac{16}{3}\int_0^v \frac{\partial \hat{F}_s}{\partial w}(w, Q^2)\ln(1 - e^{w-v})dw \\ &\quad - \frac{8}{3}\int_0^v \hat{F}_s(w, Q^2)(e^{-(v-w)} + e^{-2(v-w)})dw \\ &\quad + 2n_f x\int_0^v \hat{G}(w, Q^2)(e^{-(v-w)} - 2e^{-2(v-w)} \\ &\quad + 2e^{-3(v-w)})dw, \end{aligned} \tag{7}$$

$$\begin{aligned}&\frac{4\pi}{\alpha_s(Q^2)}\frac{\partial \hat{G}}{\partial \ln Q^2}(v, Q^2) \\ &= \frac{33 - 2n_f}{3}\hat{G}(v, Q^2) + 12\int_0^v \frac{\partial \hat{G}}{\partial w}(w, Q^2)\ln(1 - e^{-(v-w)})dw \\ &\quad + 12\int_0^v \hat{G}(w, Q^2)(1 - 2e^{-(v-w)} \\ &\quad + e^{-2(v-w)} - e^{-3(v-w)})dw \\ &\quad + \frac{8}{3}\int_0^v \hat{F}_s(w, Q^2)(1 + (1 - e^{-(v-w)})^2)dw. \end{aligned} \tag{8}$$

The DGLAP equations have now been written in a form such that all of the integrals in Eqs. (7) and (8) are manifestly seen to be convolution integrals. Thus, introducing Laplace transforms allows us to factor these convolution integrals, since the Laplace transform of a convolution is the product of the Laplace transforms of the factors, i.e.,

$$\begin{aligned}\mathcal{L}\left[\int_0^v F[w]H[v - w]dw; s\right] &= \mathcal{L}\left[\int_0^v F[v - w]H[w]dw; s\right] \\ &= \mathcal{L}[F[v]; s] \times \mathcal{L}[H[v]; s]. \end{aligned} \tag{9}$$

Defining the Laplace transforms of $\hat{F}_s(v, Q^2)$ and $\hat{G}(v, Q^2)$ in s space as

$$\begin{aligned}f(s, Q^2) &\equiv \mathcal{L}[\hat{F}_s(v, Q^2); s] = \int_0^\infty \hat{F}_s(v, Q^2)e^{-sv}dv, \\ g(s, Q^2) &\equiv \mathcal{L}[\hat{G}(v, Q^2); s] = \int_0^\infty \hat{G}(v, Q^2)e^{-sv}dv \end{aligned} \tag{10}$$

and noting that

$$\begin{aligned}\mathcal{L}\left[\frac{\partial \hat{F}_s}{\partial w}(w, Q^2); s\right] &= sf(s, Q^2), \\ \mathcal{L}\left[\frac{\partial \hat{G}}{\partial w}(w, Q^2); s\right] &= sg(s, Q^2), \end{aligned} \tag{11}$$

since $F_s(v = 0, Q^2) = G(v = 0, Q^2) = 0$, we now factor the Laplace transforms of Eqs. (7) and (8) into two coupled first-order differential equations in Laplace space s having Q^2-dependent coefficients. These can be written as

$$\begin{aligned}\frac{\partial f}{\partial \ln Q^2}(s, Q^2) &= \frac{\alpha_s(Q^2)}{4\pi}\Phi_f(s)f(s, Q^2) \\ &\quad + \frac{\alpha_s(Q^2)}{4\pi}\Theta_f(s)g(s, Q^2), \end{aligned} \tag{12}$$

$$\begin{aligned}\frac{\partial g}{\partial \ln Q^2}(s, Q^2) &= \frac{\alpha_s(Q^2)}{4\pi}\Phi_g(s)g(s, Q^2) \\ &\quad + \frac{\alpha_s(Q^2)}{4\pi}\Theta_g(s)f(s, Q^2). \end{aligned} \tag{13}$$

The coefficient functions Φ and Θ are given by

$$\Phi_f(s) = 4 - \frac{8}{3}\left(\frac{1}{s + 1} + \frac{1}{s + 2} + 2(\psi(s + 1) + \gamma_E)\right), \tag{14}$$

$$\Theta_f(s) = 2n_f\left(\frac{1}{s + 1} - \frac{2}{s + 2} + \frac{2}{s + 3}\right), \tag{15}$$

$$\begin{aligned}\Phi_g(s) &= \frac{33 - 2n_f}{3} + 12\left(\frac{1}{s} - \frac{2}{s + 1} + \frac{1}{s + 2} - \frac{1}{s + 3}\right. \\ &\quad \left. - \psi(s + 1) - \gamma_E\right), \end{aligned} \tag{16}$$

$$\Theta_g(s) = \frac{8}{3}\left(\frac{2}{s} - \frac{2}{s + 1} + \frac{1}{s + 2}\right), \tag{17}$$

where $\psi(x)$ is the digamma function and $\gamma_E = 0.577\,215\,6\ldots$ is Euler's constant.

The solution of the coupled equations in Eqs. (12) and (13) in terms of initial values of the functions f and g, specified as functions of s at virtuality Q_0^2, is straightforward. The Q^2 dependence of the solutions is expressed entirely through the function

$$\tau(Q^2, Q_0^2) = \frac{1}{4\pi}\int_{Q_0^2}^{Q^2} \alpha_s(Q'^2) d\ln Q'^2. \tag{18}$$

With the initial conditions $f_0(s) \equiv f(s, Q_0^2)$ and $g_0(s) \equiv g(s, Q_0^2)$, the solutions are

$$f(s,\tau) = k_{ff}(s,\tau) f_0(s) + k_{fg}(s,\tau) g_0(s), \tag{19}$$

$$g(s,\tau) = k_{gg}(s,\tau) g_0(s) + k_{gf}(s,\tau) f_0(s), \tag{20}$$

where the coefficient functions in the solution are

$$k_{ff}(s,\tau) \equiv e^{(\tau/2)(\Phi_f(s)+\Phi_g(s))}\left[\cosh\left(\frac{\tau}{2}R(s)\right) + \frac{\sinh(\frac{\tau}{2}R(s))}{R(s)}(\Phi_f(s) - \Phi_g(s))\right], \tag{21}$$

$$k_{fg}(s,\tau) \equiv e^{(\tau/2)(\Phi_f(s)+\Phi_g(s))}\frac{2\sinh(\frac{\tau}{2}R(s))}{R(s)}\Theta_f(s), \tag{22}$$

$$k_{gg}(s,\tau) \equiv e^{(\tau/2)(\Phi_f(s)+\Phi_g(s))}\left[\cosh\left(\frac{\tau}{2}R(s)\right) - \frac{\sinh(\frac{\tau}{2}R(s))}{R(s)}(\Phi_f(s) - \Phi_g(s))\right], \tag{23}$$

$$k_{gf}(s,\tau) \equiv e^{(\tau/2)(\Phi_f(s)+\Phi_g(s))}\frac{2\sinh(\frac{\tau}{2}R(s))}{R(s)}\Theta_g(s), \tag{24}$$

with $R(s) \equiv \sqrt{(\Phi_f(s) - \Phi_g(s))^2 + 4\Theta_f(s)\Theta_g(s)}$. Clearly, the fundamental solutions in Laplace space s, Eqs. (19) and (20), are symmetric under the interchange $f \leftrightarrow g$.

Let us now define four kernels K_{FF}, K_{FG}, K_{GF}, and K_{GG}, the inverse Laplace transforms of the k's, i.e.,

$$\begin{aligned} K_{FF}(\upsilon,\tau) &\equiv \mathcal{L}^{-1}[k_{ff}(s,\tau);\upsilon], \\ K_{FG}(\upsilon,\tau) &\equiv \mathcal{L}^{-1}[k_{fg}(s,\tau);\upsilon], \end{aligned} \tag{25}$$

$$\begin{aligned} K_{GG}(\upsilon,\tau) &\equiv \mathcal{L}^{-1}[k_{gg}(s,\tau);\upsilon], \\ K_{GF}(\upsilon,\tau) &\equiv \mathcal{L}^{-1}[k_{gf}(s,\tau);\upsilon]. \end{aligned} \tag{26}$$

It is evident from Eqs. (18), (22), and (24) that K_{FG} and K_{GF} vanish for $Q^2 = Q_0^2$, where $\tau(Q^2, Q_0^2) = 0$. It can also be shown without difficulty that for $\tau = 0$, $K_{FF}(\upsilon, 0) = K_{GG}(\upsilon, 0) = \delta(\upsilon)$ and $K_{FG}(\upsilon, 0) = K_{GF}(\upsilon, 0) = 0$.

The initial boundary conditions at Q_0^2 are given by $F_{s0}(x) = F_s(x, Q_0^2)$ and $G_0(x) = G(x, Q_0^2)$. In υ space, $\hat{F}_{s0}(\upsilon) \equiv F_{s0}(e^{-\upsilon})$ and $\hat{G}_0(\upsilon) \equiv G_0(e^{-\upsilon})$ are the inverse Laplace transforms of $f_0(s)$ and $g_0(s)$, respectively, i.e.,

$$\hat{F}_{s0}(\upsilon) \equiv \mathcal{L}^{-1}[f_0(s);\upsilon] \quad \text{and} \quad \hat{G}_0(\upsilon) \equiv \mathcal{L}^{-1}[g_0(s);\upsilon]. \tag{27}$$

Finally, we can write our *decoupled* singlet structure function $\hat{F}_s$ and $\hat{G}$ solutions in υ space in terms of the convolution integrals as

$$\hat{F}_s(\upsilon, Q^2) = \int_0^\upsilon K_{FF}(\upsilon - w, \tau(Q^2, Q_0^2))\hat{F}_{s0}(w)dw + \int_0^\upsilon K_{FG}(\upsilon - w, \tau(Q^2, Q_0^2))\hat{G}_0(w)dw, \tag{28}$$

$$\hat{G}(\upsilon, Q^2) = \int_0^\upsilon K_{GG}(\upsilon - w, \tau(Q^2, Q_0^2))\hat{G}_0(w)dw + \int_0^\upsilon K_{GF}(\upsilon - w, \tau(Q^2, Q_0^2))\hat{F}_{s0}(w)dw. \tag{29}$$

We now derive an alternate form of the solution to the decoupled equation, very useful for computational purposes, that does not use the convolution theorem. Using a suitable fast and accurate numerical inverse Laplace transform [12], we can directly invert Eqs. (19) and (20), since $f_0(s)$ and $g_0(s)$—the Laplace transforms of the known starting functions $\hat{F}_{s0}(\upsilon, Q^2)$ and $\hat{G}_0(\upsilon, Q^2)$—are readily obtainable; the coefficient functions, the k's given in Eqs. (21)–(24), are known functions of s and τ, and hence, of Q^2 and Q_0^2. Thus we finally write our decoupled analytic solution in υ space as

$$\hat{F}_s(\upsilon, Q^2) = \mathcal{L}^{-1}[(k_{ff}(s,\tau)f_0(s) + k_{fg}(s,\tau)g_0(s));\upsilon], \tag{30}$$

$$\hat{G}(\upsilon, Q^2) = \mathcal{L}^{-1}[(k_{gg}(s,\tau)g_0(s) + k_{gf}(s,\tau)f_0(s));\upsilon]. \tag{31}$$

In order to use our solution in the integral representation of Eqs. (28) and (29), we must first numerically invert Laplace transforms of the types k_{ff} and k_{gg} that for small τ look similar to Dirac δ functions—a formidable numerical task that is inherently inaccurate, and is thus computationally intensive and significantly slower (but possible) using the numerical inverse transforms of Ref. [13]. On the other hand, if we use Eqs. (30) and (31), we only have to invert a function whose inverse Laplace transform $[\hat{F}_s(\upsilon, Q^2)$ or $\hat{G}(\upsilon, Q^2)]$ is very smooth and thus can be well approximated by a high order polynomial in υ. As shown in Ref. [13], it can then, in principle, be evaluated to arbitrary accuracy very rapidly. It will be shown in the Appendix that we actually achieve a fractional accuracy of $O(10^{-11})$ in our numerical Laplace inversion. In Sec. VI we will do a detailed evaluation of the inherent overall

numerical accuracy for actual physical problems, showing that we can do both devolution and evolution rapidly to fractional accuracies of $O(10^{-9})$ using the numerical methods outlined in the Appendix.

The final desired decoupled $F_s(x, Q^2)$ and $G(x, Q^2)$ in Bjorken x space are readily found by substituting $\upsilon = \ln(1/x)$ into the υ-space solutions for $\hat{F}_s(\upsilon, Q^2)$ and $\hat{G}(\upsilon, Q^2)$ from Eqs. (30) and (31).

III. ANALYTIC LO NONSINGLET DISTRIBUTIONS

For *nonsinglet* distributions $F_{ns}(x, Q^2)$, such as the difference between the u and d quark distributions, $x[u(x, Q^2) - d(x, Q^2)]$, we can schematically write the logarithmic derivative of F_{ns} as the convolution of $F_{ns}(x, Q^2)$ with the nonsinglet splitting function $\mathcal{K}_{ns}(x)$ (using the convolution symbol $\otimes$), i.e.,

$$\frac{4\pi}{\alpha_s(Q^2)} \frac{\partial F_{ns}}{\partial \ln(Q^2)}(x, Q^2) = F_{ns} \otimes \mathcal{K}_{ns}. \tag{32}$$

After again changing to the variable $\upsilon = \ln(1/x)$ and going to Laplace space s, we find the simple solution

$$\begin{aligned} f_{ns}(s, \tau) &= e^{\tau \Phi_{ns}(s)} f_{ns0}(s), \qquad \text{where} \\ \Phi_{ns}(s) &= \mathcal{L}[e^{-\upsilon} \hat{\mathcal{K}}_{ns}(\upsilon); s] \quad \text{and} \\ \hat{\mathcal{K}}_{ns}(\upsilon) &= \mathcal{K}_{ns}(e^{-\upsilon}). \end{aligned} \tag{33}$$

Thus we can find *any* nonsinglet solution in υ space, using the nonsinglet kernel $K_{ns}(\upsilon) \equiv \mathcal{L}^{-1}[e^{\tau \Phi_{ns}(s)}; \upsilon]$, by employing either the Laplace convolution relation

$$F_{ns}(\upsilon, Q^2) = \int_0^{\upsilon} K_{ns}(\upsilon - w, \tau(Q^2, Q_0^2)) \hat{F}_{ns0}(w) dw \tag{34}$$

or the nonintegral form

$$F_{ns}(\upsilon, Q^2) = \mathcal{L}^{-1}[e^{\tau \Phi_{ns}(s)} f_{ns0}(s); \upsilon]. \tag{35}$$

In this case, either method works equally well numerically, since the nonsinglet functions $K_{ns}(\upsilon)$ can also be approximated by a polynomial in υ.

For brevity, we will not pursue the case of the nonsinglet solution any further here except to note that in LO the $\Phi_{ns}(s)$ in Eq. (33) is identical to $\Phi_f(s)$ defined in Eq. (14). Instead, we will concentrate on the more difficult case of F_s and G.

IV. LO MSTW2008 SINGLET AND GLUON DISTRIBUTIONS

As an example of the application of our analytic decoupled solutions, we will use the published MSTW2008 initial starting functions $F_{s0}(x)$ and $G_0(x)$ at $Q_0^2 = 1$ GeV^2 [4] and will compare our LO x-space gluon distribution $G(x, Q^2) = xg(x, Q^2)$ using Eq. (31) and our LO singlet structure function $F_s(x, Q^2)$ using Eq. (30)—both numerically evaluated using a powerful new inverse Laplace transformation algorithm [12]—with the corresponding LO distributions published by the MSTW Collaboration [4]. In order to insure continuity across the boundaries $Q^2 = M_c^2$ and M_b^2, we will first evolve from $Q_0^2 = 1$ GeV^2 (the MSTW Q_0^2 value) to M_c^2 and use our evolved values of $G(x, M_c^2)$ and $F_s(x, M_c^2)$ for *new* starting values $G_0(x)$ and $F_{s0}(x)$. We will then evolve to M_b^2, repeating the process, thus insuring continuity of G and F_s at the boundaries where n_f changes. We use the MSTW values $M_c = 1.40$ GeV, $M_b = 4.75$ GeV, $\alpha_s(1\text{ GeV}^2) = 0.6818$, and $\alpha_s(M_Z^2) = 0.139\,39$ in their definition of $\alpha_s(Q^2)$ in Eq. (4).

A. $G(x, Q^2)$ and $Fs(x, Q^2)$ for LO MSTW2008

In Fig. 1 we show the LO x-space results for $G(x, Q^2) = xg(x, Q^2)$ (upper figure) and $F_s(x, Q^2)$ (lower figure) vs x,

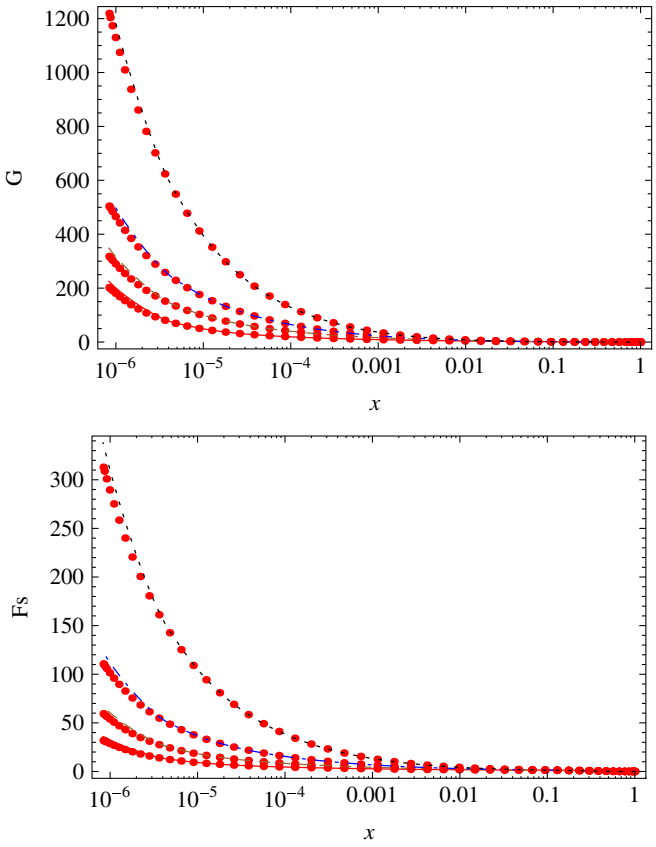

FIG. 1 (color online). Plots for LO MSTW2008 [4] gluon distributions $G(x, Q^2) = xg(x, Q^2)$ (upper plot) and $F_s(x, Q^2)$ distributions (lower plot) vs Bjorken x. The MSTW2008 curves are for $Q^2 = 5$, 20, 100, and M_Z^2 GeV^2, bottom to top. The (red) dots are our evolution results for LO $G(x, Q^2)$ from Eq. (31) and F_s from Eq. (30), after converting to x space, using the LO MSTW2008 [4] values for $F_{s0}(x)$ and $G_0(x)$, with their choice of $Q_0^2 = 1$ GeV^2. The x range covers all of the published LO MSTW2008 x data.

for four representative values of Q^2. The x domain, $10^{-6} \leq x \leq 1$, is the complete region covered by the MSTW group [4]. The curves are the published LO MSTW2008 distributions [4]: from bottom to top, the (red) curve is for $Q^2 = 5$ GeV^2, the (brown) dashed curve is for $Q^2 = 20$ GeV^2, the (blue) dot-dashed curve is for $Q^2 = 100$ GeV^2, and the (black) dotted curve is for $Q^2 = M_Z^2$. The (red) dots are our analytic results for LO $G(x, Q^2)$ from Eq. (31) and $F_s(x, Q^2)$ from Eq. (30), converted to x space, using the LO MSTW2008 values for $F_{s0}(x)$ and $G_0(x)$; the numerical values were evaluated using MATHEMATICA [15]. An outline of the numerical procedure is given in the Appendix.

For large x, the agreement is excellent for all Q^2. However, as seen in a close inspection of Fig. 1, the disagreement for both G and F_s becomes significantly large as we go to small x. We will explore this in detail in Sec. IV B.

B. Accuracy of evolved LO MSTW2008 distributions

We now investigate quantitatively the accuracy of the *evolved* LO MSTW2008 distributions ($Q^2 > Q_0^2$), introducing the fractional accuracy variable

$$\text{fractional accuracy} \equiv 1 - f_{i,\text{BDHM}}/f_{i,\text{MSTW}}, \qquad i = 1, 2, \tag{36}$$

where $f_1 = F_s$, $f_2 = G$, with BDHM denoting our LO analytic evaluations and MSTW denoting the published LO MSTW2008 values [4]. We show in Fig. 2 the fractional accuracy for the LO MSTW published distributions [4] $G(x, Q^2)$ (upper figure) and $F_s(x, Q^2)$ (lower figure) using the same four Q^2 values and legends used in Sec. IV and Fig. 1; i.e., the (red) curves are $Q^2 = 5$ GeV^2, the (brown) dashed curves are $Q^2 = 20$ GeV^2, the (blue) dot-dashed curves are $Q^2 = 100$ GeV^2, and the (black) dotted curves are M_Z^2. Both the MSTW2008 G and F_s are in excellent agreement with our (much more numerically precise) calculations in the domain $x \gtrsim 10^{-4}$, with a fractional accuracy of $\sim$0.1–0.5%. However, as is clearly seen in Fig. 1 for *both* G and F_s and for *all* Q^2, there is the same inaccuracy pattern in x, an increase of the fractional accuracy to $\sim$2% down to $x \approx 8 \times 10^{-6}$, followed by a dip at $x \approx 4 \times 10^{-6}$, with a final rise to another maximum at $x \approx 2 \times 10^{-6}$ whose fractional accuracy is $\sim$12%. These final inaccuracies at small x are quite significant. Since the x patterns are essentially independent of whether we are evaluating either G or F_s, as well as being independent of Q^2, they suggest that the MSTW numerical program undergoes a significant structural change at some unique value of x, independent of Q^2, that seriously degrades their numerical output, leading to large errors at small x. The largest errors occur at the smallest Q^2; at Q_0^2 (not shown) the error is $\sim$12%–13%, and decreases monotonically to $\sim$4%–5% at the highest Q^2. As we will later see in Sec. V, there is no such pattern in the LO CTEQ6L data [5].

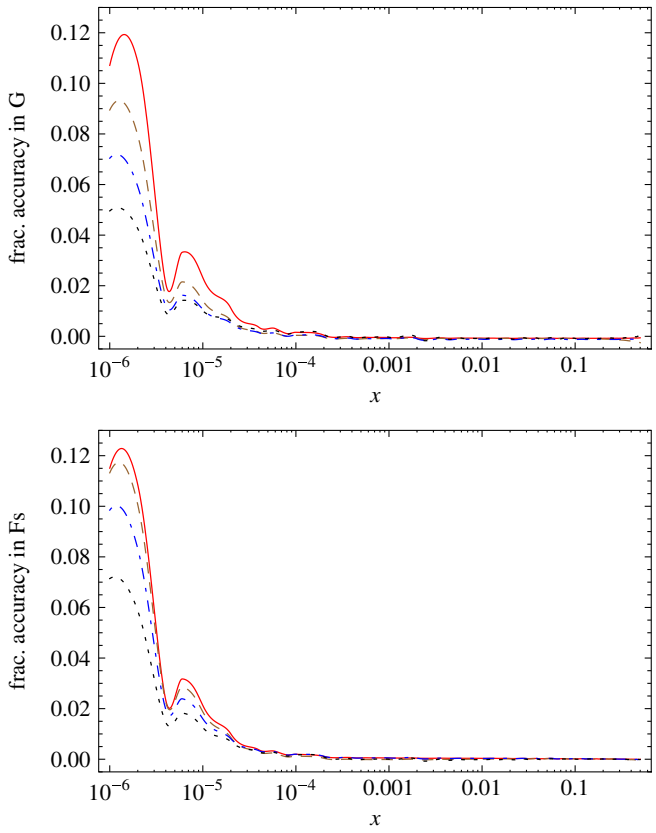

FIG. 2 (color online). Fractional accuracy plots for LO MSTW [4] gluon distributions $G(x, Q^2) = xg(x, Q^2)$ (upper plot) and $F_s(x, Q^2)$ distributions (lower plot), for $Q^2 = 5$, 20, 100, and M_Z^2 GeV^2, where the fractional accuracy is given by Eq. (36). The (red) curves are $Q^2 = 5$ GeV^2, the (brown) dashed curves are $Q^2 = 20$ GeV^2, the (blue) dot-dashed curves are $Q^2 = 100$ GeV^2, and the (black) dotted curves are M_Z^2. The x range covers all of the published LO MSTW x data.

V. LO CTEQ6L SINGLET AND GLUON DISTRIBUTIONS

As a second example of the application of our analytic decoupled solutions, we will compare our LO x-space gluon distribution $G(x, Q^2) = xg(x, Q^2)$ from Eq. (31) and our LO singlet distribution function $F_s(x, Q^2)$ from Eq. (30)—using the published LO CTEQ6L [5] initial conditions at $Q_0^2 = 1.69$ GeV^2—with the corresponding LO CTEQ6L distributions [5]. In order to insure continuity across the boundary M_b^2, we will first evolve from $Q_0^2 = 1.69$ GeV^2 (the CTEQ6L Q_0^2 value) to M_b^2 and use our evolved values of $G(x, M_c^2)$ and $F_s(x, M_c^2)$ for *new* starting values $G_0(x)$ and $F_{s0}(x)$, thus insuring continuity of G and F_s at the boundary where n_f changes. We use the CTEQ6L values $M_c = 1.3$ GeV and $M_b = 4.5$ GeV. Here we use a NLO version of $\alpha_s(Q^2)$, with $\alpha_s(M_Z^2) = 0.118$, made continuous at M_b and M_c, that was utilized in CTEQ6L (for details see Ref. [5]).

A. $G(x, Q^2)$ and $Fs(x, Q^2)$ for LO CTEQ6L

In Fig. 3 we show the Bjorken x-space results for LO $G(x, Q^2) = xg(x, Q^2)$ (upper figure) and LO $F_s(x, Q^2)$ (lower figure) vs x, for five representative values of Q^2. The x domain, $10^{-6} \leq x \leq 1$, is the complete region covered by the CTEQ group [5]. The curves are the published CTEQ6L [5] LO distributions. From bottom to top, the (red) curve is for $Q^2 = 10$ GeV^2, the (brown) dashed curve is for $Q^2 = 22$ GeV^2, the (blue) dot-dashed curve is for $Q^2 = 90$ GeV^2, the (black) dotted curve is for $Q^2 = 1200$ GeV^2, and the (orange) curve is for $Q^2 = M_Z^2$. Since CTEQ6L [5] started evolution at $Q_0^2 = 1.69$ GeV^2, we used F_{s0} and G_0 constructed from their values at $Q_0^2 = 1.69$ GeV^2 in Eqs. (30) and (31). The (red) dots are our results for LO $G(x, Q^2)$ from Eq. (31) and $F_s(x, Q^2)$ from Eq. (30) converted to x space, using LO CTEQ6L values for $F_{s0}(x)$ and $G_0(x)$, evaluated using MATHEMATICA [15].

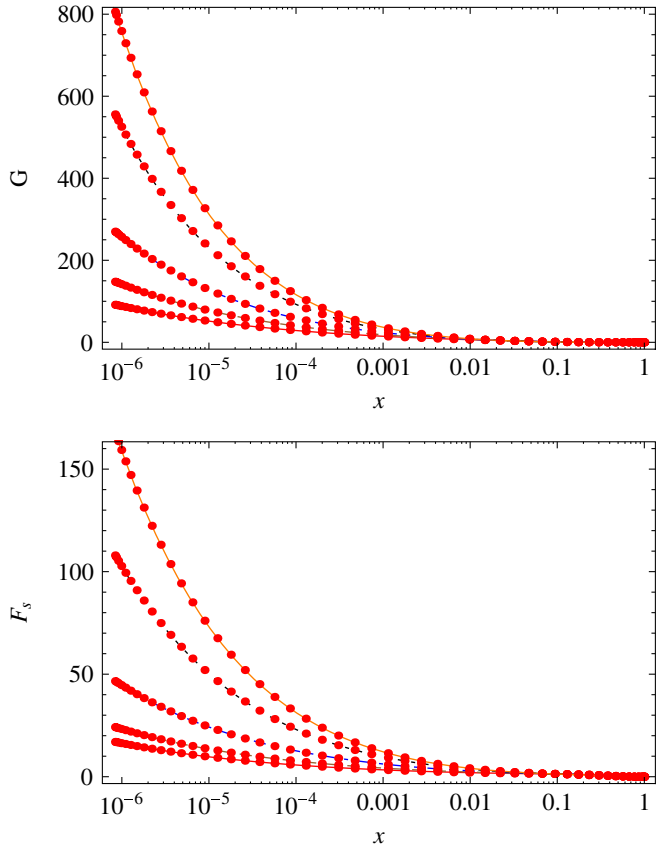

FIG. 3 (color online). Plots for LO CTEQ6L [5] gluon distributions $G(x, Q^2) = xg(x, Q^2)$ (upper plot) and $F_s(x, Q^2)$ distributions (lower plot) vs Bjorken x. The curves are for $Q^2 = 10$, 22, 90, 1200, and M_Z^2 GeV^2, bottom to top. The (red) dots are our evolution results for LO $G(x, Q^2)$ from Eq. (31) and F_s from Eq. (30) (converted to x space) using the LO CTEQ6L values for $F_{s0}(x)$ and $G_0(x)$, where $Q_0^2 = 1.69$ GeV^2. The x range in this figure covers all of the published LO CTEQ6L x data.

For all Q^2 the agreement is excellent over the entire x region, with a fractional accuracy of about $\pm 5 \times 10^{-4}$ (completely consistent with the four significant figures that are published)—for all F_s and G at the five virtualities that we evaluated—with a minor and numerically unimportant exception of the lowest x region of $F_s(x, Q^2 = 22)$, where there was an *offset* of $\approx 2 \times 10^{-3}$.

B. Accuracy of CTEQ6L devolved distributions

In Fig. 3, all of the distributions were for evolutions of G and F_s from the CTEQ6L $Q_0^2 = 1.69$ GeV^2 to larger Q^2. For another physics investigation, not relevant to this paper, we decided to compare LO starting distributions for MRSTW2008 and CTEQ6L at the MSTW2008 starting value of $Q_0^2 = 1$ GeV^2. Using $n_f = 3$, we devolved G and F_s from the CTEQ6L starting values at $Q_0^2 = 1.69$ GeV^2 down to $Q^2 = 1$ GeV^2, the MSTW2008 starting value for Q_0^2.

The results of this devolution are compared to the published CTEQ6L values [5] in Fig. 4 for G (upper figure)

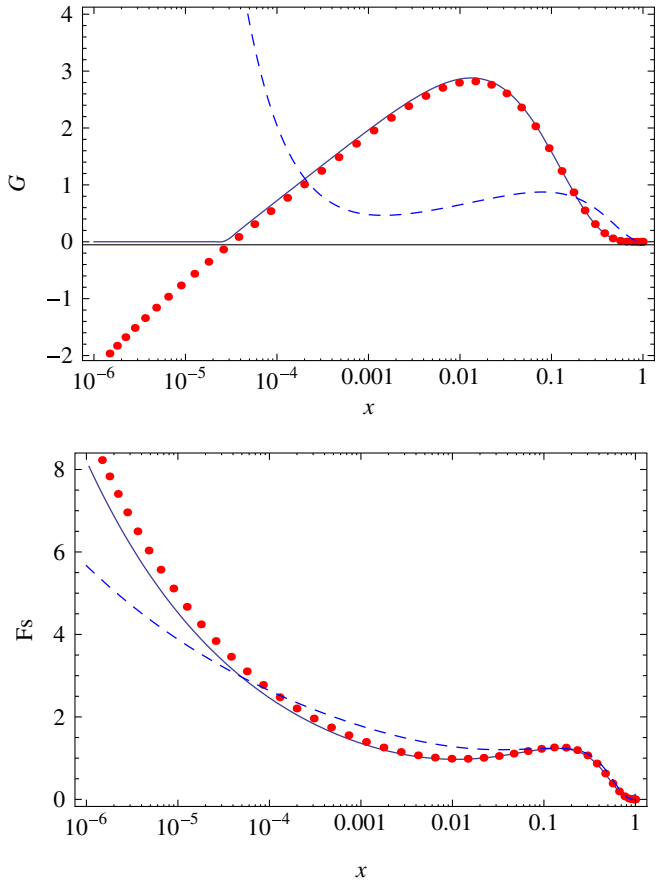

FIG. 4 (color online). Plots of gluon distributions $G(x, Q^2) = xg(x, Q^2)$ (upper plot) and $F_s(x, Q^2)$ distributions (lower plot) vs Bjorken x, at the devolved value of $Q^2 = 1$ GeV^2. The (red) dots are our devolution results, the (black) solid curves are the published CTEQ6L results [5], and the (blue) dashed curves are the starting $F_{s0}(x)$ and $G_0(x)$ for MSTW2008 [4].

and F_s (lower figure). In all cases, when we refer to "published CTEQ6L values," we mean the results found on the Durham parton distributions function generator website; see [16]. The solid (black) curves are for CTEQ6L and the (red) dots are from Eqs. (30) and (31). In marked contrast to their evolution results, the CTEQ6L devolution results are numerically unstable, with F_s being wrong by $\approx 12\%$ at $x = 10^{-6}$. We also note that there are large disagreements with their devolved $G(x)$ for small x. Clearly, they have chosen to chop off their G distribution at small x, i.e., to write $G(x) = 0$ for small x, rather than allow it to become negative. The errors for both G and F_s become insignificant as x approaches 1. It is clear that CTEQ encounters major problems with the numerical stability of its published results for $Q^2 < Q_0^2$, whereas they are completely accurate for $Q^2 > Q_0^2$.

For comparison, we also show in Fig. 4 the published MSTW2008 starting distributions [4] $G_0(x)$ and $F_{s0}(x)$ at $Q_0^2 = 1$ GeV^2, the dashed (blue) curves. We note that the LO gluon distributions of the two different collaborations, when evaluated at the *same* virtuality, $Q^2 = 1$ GeV^2, bear little or no resemblance to each other, with the CTEQ6L gluon distribution going *negative* for $x \lesssim 3 \times 10^{-5}$. Although both singlet structure functions $F_s(x, Q^2 = 1)$ stay positive—as they must—Fig. 4 shows that there are also large differences between the two singlet structure functions at low x.

VI. OVERALL NUMERICAL ACCURACY OF ANALYTICAL DEVOLUTION AND EVOLUTION

As mentioned in Sec. V B, we had *devolved* from $Q_0^2 = 1.69$ GeV^2 to $Q^2 = 1$ GeV^2, using the known CTEQ6L $G_0(x)$ and $F_{s0}(x)$ starting values. To estimate the *overall* accuracy of our entire numerical procedure, we took our devolved distributions $G(x, Q^2 = 1)$ and $F_s(x, Q^2 = 1)$ and used *them* as starting values so that we could again evolve back to $Q^2 = 1.69$ GeV^2. Finally, we compared the evolved numerical results with the original $F_{s0}(x)$ and $G_0(x)$, the distributions that we started with at $Q^2 = 1.69$ GeV^2. An outline of our entire numerical procedure is given in the Appendix.

In Fig. 5, we show the fractional accuracy of this "round-trip" comparison. The upper figure is for G and the lower figure is for F_s. The (red) dots are the round-trip fractional accuracies at discrete x values chosen to start and end this numerical exercise (corresponding to the transformed zeros of the Chebyshev polynomials that we discuss in the Appendix). For the visual convenience of the reader, we have connected the dots.

Where either G or F_s is significantly large ($x \lesssim 0.3$), we see that the round-trip error is $\lesssim 4 \times 10^{-9}$, thus yielding an overall error estimate of $\lesssim \pm 2 \times 10^{-9}$ for either evolution or devolution. Detailed causes for this error are discussed in the Appendix.

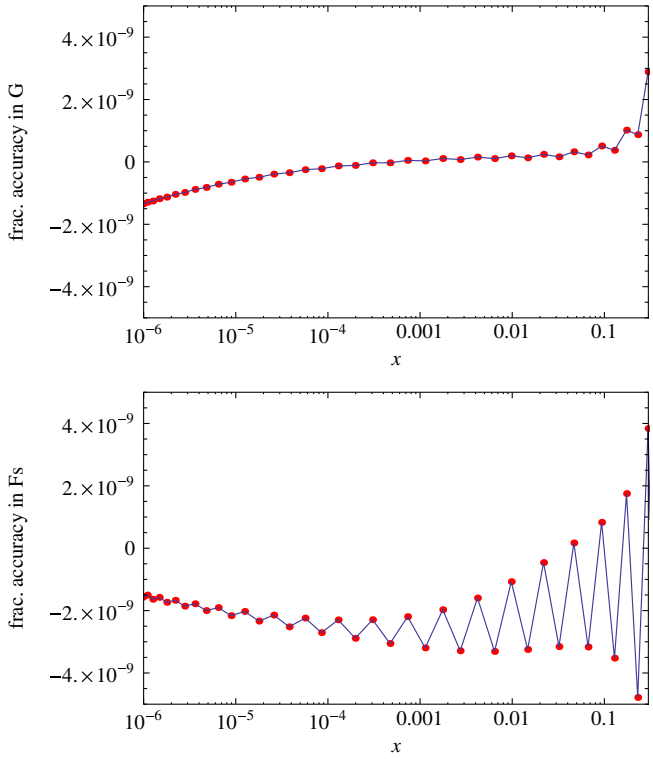

FIG. 5 (color online). Fractional accuracy plots for our LO gluon distributions $G(x, Q^2) = xg(x, Q^2)$ (upper figure) from Eq. (31) and $F_s(x, Q^2)$ distributions (lower figure) from Eq. (30). These accuracy estimates resulted from devolution from $Q_0^2 = 1.69$ GeV^2 to $Q^2 = 1$ GeV^2 then, using these results for evolution, back to $Q^2 = 1.69$ GeV^2. The fractional value error estimates result from comparing the original values with the devolved-evolved ones.

It is gratifying that the overall numerical uncertainty in our LO analytically decoupled solutions is small, thus furnishing us not only with a new, accurate and fast calculation tool for exploring the effects of the shapes of different starting value distributions, but also with a diagnostic tool for easily determining the numerical calculational reliability of the already published parton distribution functions that are currently in major use by the high energy physics community.

VII. CONCLUSIONS

In conclusion, we have constructed decoupled analytical solutions for $F_s(x, Q^2)$ and $G(x, Q^2)$ from the coupled LO DGLAP equations, yielding accurate numerical results for *both* evolution and devolution of $O(10^{-9})$—a fast tool to study the dependence on the shape of the starting distributions $F_{s0}(x)$ and $G_0(x)$, the boundary conditions at the starting value Q_0^2. Similar procedures can be used for nonsinglet distributions, allowing one to obtain analytic LO solutions for individual quark distributions, as well as for the gluon distribution; thus avoiding the necessity for purely numerical solutions of the coupled DGLAP

equations on a giant two-dimensional grid in (x, Q^2) space. In essence, using a program such as MATHEMATICA [15], we can now define a parton distribution function for each quark and gluon and—after inputting the desired x and Q^2—evaluate it accurately and rapidly [for a fast MATHEMATICA program calculating LO $F_s(x, Q^2)$ and $G(x, Q^2)$, see the Appendix].

We have also used our analytic solutions coupled with the MSTW2008 initial starting functions [4] as a new and powerful diagnostic tool to study the numerical accuracy (the computational accuracy of their evolution code) of the LO MSTW2008 published distributions [4]. For the small x region, $x \lesssim 10^{-4}$, we discovered a pattern of significant numerical (computational) errors for both F_s and G, ranging up to $\approx 12\%$ at the smallest x values in the published MSTW2008 results [4], true for all Q^2.

Applying the same new tools to CTEQ6L, we found no errors (to their accuracy of four significant figures) in either F_s or G values when they did evolution from $Q_0^2 = 1.69\ \mathrm{GeV}^2$ to higher Q^2 values, but significant errors—increasing with decreasing x—when they did devolution to smaller Q^2.

In the future, we intend to evaluate $F_{s0}(x)$ and $G_0(x)$ in both LO and NLO, from a fit to small x experimental data for the structure function $F_2^{\gamma p}(x, Q^2)$, in order to obtain (analytically) accurate values of $G(x, Q^2)$ directly tied to experiment, which are needed for the interpretation of experiments at the LHC.

ACKNOWLEDGMENTS

The authors would like to thank the Aspen Center for Physics for its hospitality during the time parts of this work were done. P. Ha would like to thank Towson University, Fisher College of Science and Mathematics for travel support. D. W. M. received support from DOE Grant No. DE-FG02-04ER41308.

APPENDIX

We outline here the actual calculation procedures necessary for fast and accurate numerical evaluations of Eqs. (30) and (31). These calculations, although robust, require delicate choices as to the numerical techniques used in evaluating Eqs. (30) and (31).

As shown in Ref. [12], if the function $g(s)$ goes to 0 at ∞ more rapidly than $1/s$, then we can accurately approximate its inverse Laplace transform $G(\upsilon)$ by

$$G(\upsilon) \approx -\frac{2}{\upsilon} \sum_{i=1}^{N} \mathrm{Re}[\omega_i g(\alpha_i/\upsilon)], \tag{A1}$$

where $2N$ is the order of the approximation, and ω_i and α_i, $i = 1, 2, \ldots, 2N$, are known complex numbers for a given $2N$, occurring in complex conjugate pairs. The actual numerical evaluation of Eq. (A1) can be quite unstable if one does not utilize arbitrary accuracy arithmetic as discussed in Ref. [12], since the weight functions ω_i become exceedingly large, even for modest $2N$, and oscillate in sign [12]. The use of MATHEMATICA (or similar programs, which also carry out arithmetical operations to arbitrary accuracy) makes this requirement easy to satisfy.

As shown in Ref. [12], the inverse Laplace transform approximation to $G(\upsilon)$ is exact if $G(\upsilon)$ is a polynomial in υ of order $4N - 1$ or less. For our purposes here, $G(\upsilon)$ in Eq. (A1) is either the $\hat{F}_s(\upsilon, Q^2)$ or the $\hat{G}(\upsilon, Q^2)$ on the left-hand side of Eq. (30) or Eq. (31), whereas $g(s)$ in Eq. (A1) is the surrogate for either $k_{ff}(s, \tau)f_0(s) + k_{fg}(s, \tau)g_0(s)$ found in the right-hand side of Eq. (30) or $k_{gg}(s, \tau)g_0(s) + k_{gf}(s, \tau)f_0(s)$ found in the right-hand side of Eq. (31). Since we must evaluate $g(s)$ at complex values of s, this necessarily implies that we must evaluate $f_0(s)$ and $g_0(s)$—the Laplace transforms of $\hat{F}_{s0}(\upsilon)$ and $\hat{G}_0(\upsilon)$, respectively—at complex values of s. As shown in Ref. [12], to insure numerical accuracy we must be able to evaluate $g(s)$ in Eq. (A1) to arbitrary accuracy. Thus we must know the Laplace transforms $f_0(s)$ and $g_0(s)$ analytically and *not* just as numerical integrations of the form $\int_0^\infty \hat{F}_{s0}(\upsilon)e^{-\upsilon s}d\upsilon$. The k's, the coefficient functions needed, are known analytically; the potential problem is with $f_0(s)$ and $g_0(s)$, the starting functions in Laplace space s.

The starting distribution functions normally used are *not* of the type that have analytic Laplace transforms. To get a sufficiently accurate numerical approximation to functions that *do* have analytic Laplace transforms is again a delicate numerical exercise. We found that we could do it sufficiently accurately by using an interpolating polynomial of order $n = 49$. Its 50 coefficients were determined by evaluating the original function at 50 points, distributed as the zeros of a 50th order Chebyshev polynomial, found in the interval $(-1, +1)$ and then linearly transformed to υ space to lie in the interval $0 \le \upsilon < 14$ $(1 \ge x > 0.83 \times 10^{-6})$. These points were chosen to try to minimize the maximum interpolation error. We note that even when using MATHEMATICA, caution was needed in order to obtain sufficient numerical accuracy with such a high order polynomial; it had to be evaluated using Horner's method (see Sec. 10.14 of Ref. [17]), since a straightforward evaluation of such a high order polynomial will yield numerical nonsense.

Using $2N = 38$ in Eq. (A1), we would have an *exact* result if either $\hat{F}_s(\upsilon, Q^2)$ in Eq. (30) or $\hat{G}(\upsilon, Q^2)$ in Eq. (31) were a polynomial in υ of degree 75 or less; see Ref. [12] for details. In actual practice, by comparing the results for the value of $2N = 38$—the value we used for our numerical evaluations—with very much larger values of $2N$ that we used for estimates of the exact solutions, we found that the fractional accuracy of inversion for both $\hat{F}_s(\upsilon, Q^2)$ and $\hat{G}(\upsilon, Q^2)$ was $\approx \pm 1 \times 10^{-11}$ for $\upsilon \gtrsim 0.3$. Thus, numerical inversion of the Laplace transform in either Eq. (30) or Eq. (31) contributes essentially nothing to our overall error of about $\pm 2 \times 10^{-9}$, since it is some 2 orders of magnitude

smaller. We comment that the overall error is essentially completely due to our numerical approximation of the starting functions and *not* the subsequent Laplace transforms of them. Therefore, we could readily reduce this error by using more than 50 points in our numerical approximations of the starting distributions, but this would be at the expense of more computational time and was felt to be unnecessary.

A typical time for computing the full x distribution of either $F_s(x)$ or $G(x)$ at an arbitrary Q^2—given the starting functions $F_{s0}(x)$ and $G_0(x)$ at Q_0^2—was about 15 s, basically proportional to the number of points in x used in the numerical approximations of the starting functions and to the number $2N$ used in the Laplace inversion routine. Thus, for most applications, we could easily reduce this time to several seconds, at the expense of some (perhaps unneeded) accuracy. The computations in this paper were made on a home PC, a Dell Model Studio XPS435MT, using an Intel 2.67 GHz 4 core i7 CPU, running 64 bit Windows Vista, and using MATHEMATICA7 [15] in parallel mode.

For a very fast MATHEMATICA7 (.nb) program that accurately calculates all LO MSTW2008 parton distribution functions, as well as $F_2^{\gamma p}(x)$ and $F_s(x)$ for any Q^2—using the LO MSTW starting values [4] for $F_s(x)$, $G(x)$ at $Q_0^2 = 1$ GeV^2—send an email request to mblock@northwestern.edu for MSTW.zip.

[1] V. N. Gribov and L. N. Lipatov, Sov. J. Nucl. Phys. **15**, 438 (1972).

[2] G. Altarelli and G. Parisi, Nucl. Phys. **B126**, 298 (1977).

[3] Y. L. Dokshitzer, Sov. Phys. JETP **46**, 641 (1977).

[4] A. D. Martin, W. J. Stirling, R. S. Thorne, and G. Watt, Eur. Phys. J. C **63**, 189 (2009).

[5] J. Pumplin *et al.* (CTEQ Collaboration), J. High Energy Phys. 07 (2002) 012.

[6] D. Stump, J. Huston, J. Pumplin, W. Tung, H. Lai, S. Kuhlmann, and J. Owens, J. High Energy Phys. 10 (2003) 046.

[7] W. K. Tung, H. L. Lai, A. Belyaev, J. Pumplin, D. Stump, and C.-P. Yuan, J. High Energy Phys. 02 (2007) 053.

[8] A. D. Martin, R. G. Roberts, W. J. Stirling, and R. S. Thorne, Eur. Phys. J. C **23**, 73 (2002).

[9] A. D. Martin, R. G. Roberts, W. J. Stirling, and R. S. Thorne, Phys. Lett. B **604**, 61 (2004).

[10] M. M. Block, L. Durand, and D. W. McKay, Phys. Rev. D **77**, 094003 (2008).

[11] M. M. Block, L. Durand, and D. W. McKay, Phys. Rev. D **79**, 014031 (2009).

[12] M. M. Block, Eur. Phys. J. C **65**, 1 (2010).

[13] M. M. Block, Eur. Phys. J. C **68**, 683 (2010).

[14] M. M. Block, L. Durand, P. Ha, and D. W. McKay, Eur. Phys. J. C **69**, 425 (2010).

[15] MATHEMATICA 7, a computing program from Wolfram Research, Inc., Champaign, IL, USA, www.wolfram.com (2009).

[16] http://hepdata.cedar.ac.uk/pdf/pdf3.html. The data used here were obtained in August 2010. We caution the reader that the website format has been changed recently, and that if one looks for CTEQ6L results for *any* $Q^2 < M_c^2$, the site now returns the numerical values *for* $Q^2 = M_c^2$; it functions normally for $Q^2 \geq M_c^2$.

[17] F. B. Hildebrand, *Introduction to Numerical Analysis* (Dover Publications, New York, 1987).